10.1071/CH17380_AC

Australian Journal of Chemistry

SUPPLEMENTARY MATERIAL

Application of Hole Transporting Materials as the Interlayer in Graphene Oxide/Single-Wall Carbon Nanotube Heterojunction Solar Cells

L. Yu,[A] T. Grace,[A] H. D. Pham,[B] M. Batmunkh,[A] M. Dadkhah,[A] C. Shearer,[A] P. Sonar[B] and J. Shapter[A,C]

[A]Centre for Nanoscale Science and Technology, School of Chemical and Physical Sciences, Flinders University, Bedford Park, SA 5042, Australia.

[B]School of Chemistry, Physics and Mechanical Engineering, Queensland University of Technology (QUT), Brisbane, Qld 4001, Australia.

[C]Corresponding author. Email: joe.shapter@flinders.edu.au

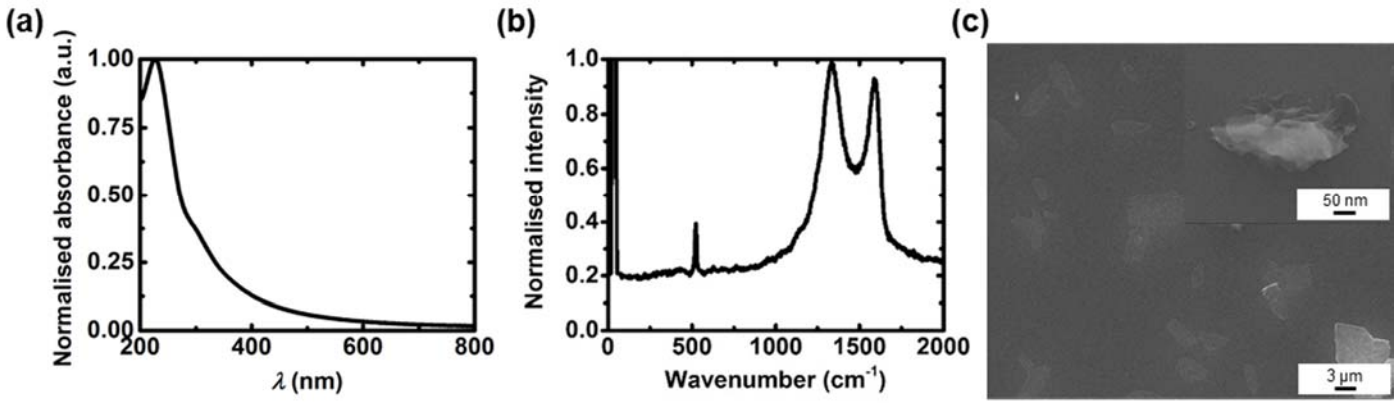

Figure S1: (a) UV-Vis of the GO stock solution (normalised at 227 nm); (b) Raman spectrum of pure GO film prepared from the stock solution (normalised at D band); (c) SEM image of GO sheets from the stock solution (the inset shows an example of GO aggregate).

There is a characteristic peak for GO at 227 nm and a broad absorbance over the visible range in the UV-Vis spectrum, as shown in **Figure S1 (a)**. The Raman spectrum shows 2 major peaks at about 1350 and 1590 cm^{-1} with the G/D band ratio below 1 (**Figure S1 (b)**), which indicates oxygen-enriched functional groups have been successfully introduced on the surface of graphene sheet. The SEM image (**Figure S1 (c)**) shows some GO flakes in the stock solution. The overall results indicate that high quality GO has been synthesised.

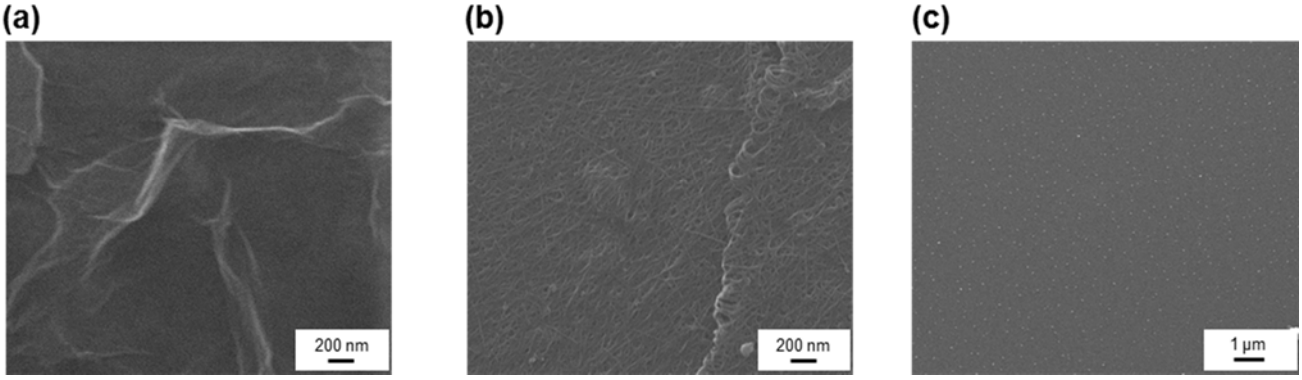

Figure S2: SEM images of (a) pure GO film on Si; (b) pure CNT film on Si; (c) drop-casted $AuCl_3$ stock solution on Si.

The SEM image of the pure GO film illustrates the wrinkle features expected for GO sheets (**Figure S2 (a)**) while there is a network of SWCNT bundles in the pure CNT film (**Figure S2 (b)**). The drop casting of $AuCl_3$ on Si introduces some AuNPs (the bright spots) over the entire area, as shown in **Figure S2 (c)**.

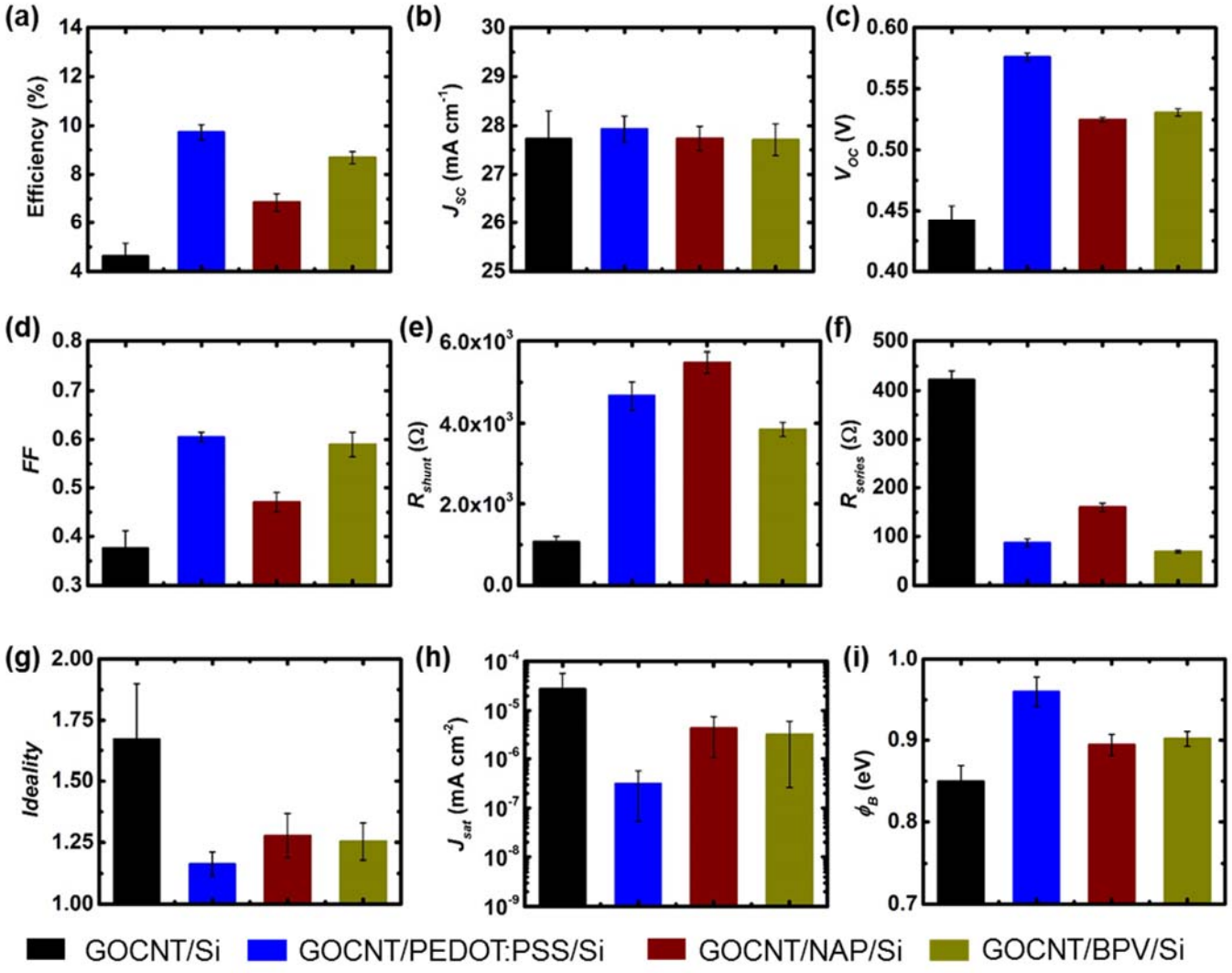

Figure S3: Details of the device performance of GOCNT/Si, GOCNT/PEDOT:PSS/Si, GOCNT/NAP/Si and GOCNT/BPV/Si; (a) Efficiency; (b) J_{sc}; (c) V_{oc}; (d) *FF*; (e) R_{shunt}; (f) R_{series}; (g) Ideality; (h) J_{sat} and (i) ϕ_B. The HTLs were applied with spin-coating at the same speed (7000 rpm) and the thickness were estimated by AFM (PEDOT:PSS: 10 nm; NAP: 30 nm; BPV; 35 nm, as shown in Figure S4, Figure S5 and Figure S6). All the devices in these plots are fabricated with as-prepared GOCNT films.

Figure S3 shows the details to the performance of GOCNT/Si and GOCNT/HTL/Si devices. The thicknesses of these HTLs are slightly different. Compared to the GOCNT/Si control devices, the GOCNT/HTL/Si devices have higher efficiency (**Figure S3 (a)**), among which GOCNT/PEDOT:PSS/Si has the highest efficiency. The performance improvement of the GOCNT/HTL/Si devices is not due to the J_{SC} but the higher V_{OC} and FF (**Figure S3 (b)-(d)**). The R_{shunt} of GOCNT/Si is at least 3 times lower than that of any type of GOCNT/HTL/Si devices while the its R_{series} is at least two times higher than those of GOCNT/HTL/Si devices, (**Figure S3 (e)** and **(f)**). In terms of the diode properties, though it is difficult to compare among GOCNT/HTL/Si devices due to the relatively large error bars, it is clear that the both the ideality and the J_{sat} of all three types of GOCNT/HTL/Si devices are lower than that of GOCNT/Si control device (**Figure S3 (g)** and **(h)**). Furthermore, the calculated ϕ_B increases with the addition of HTL between GOCNT and Si substrate (**Figure S3 (i)**).

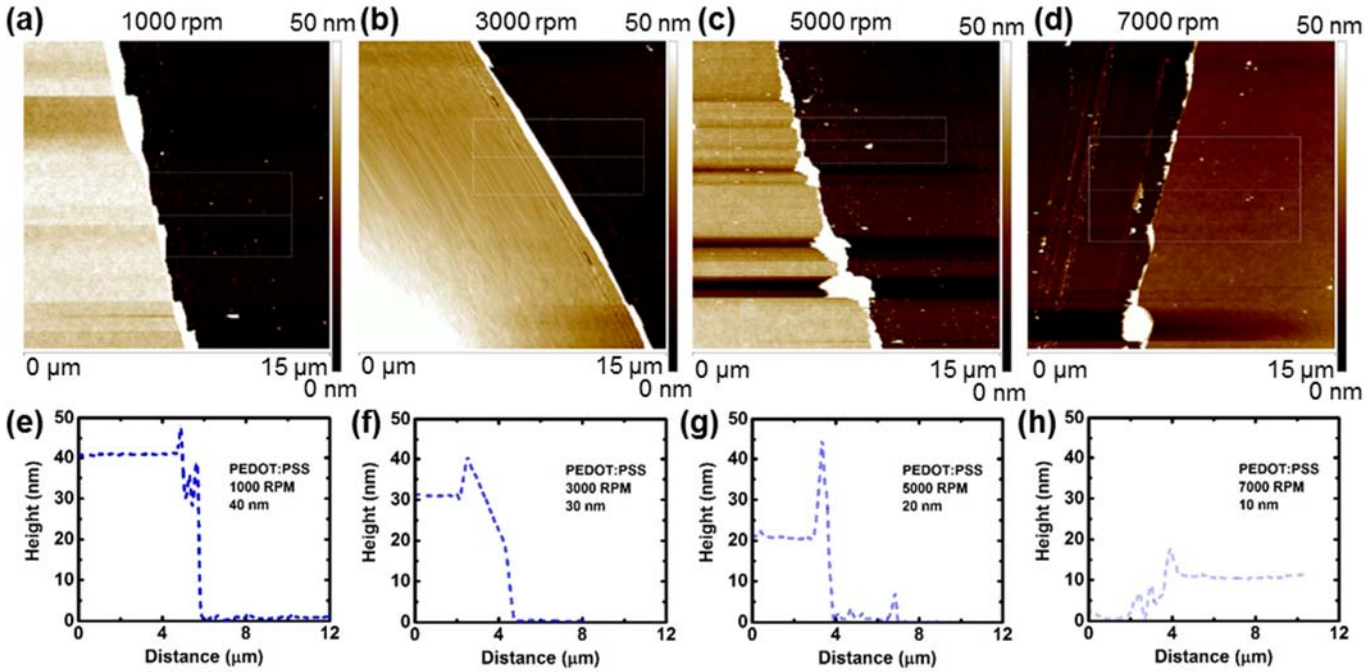

Figure S4: Topographical images ((a)-(d)) from AFM and plots of height versus distance ((e)-(h)) from the step function of NanoScope Analysis for the thickness measurement of PEDO:PSS layers on Si with different spin speed from 1000 to 7000 rpm.

Figure S4 shows the results of the AFM measurement of the thickness of PEDOT:PSS layers on Si. The thicknesses of PEDOT:PSS prepared by spin coating at 1000, 3000, 5000, and 7000 rpm are 40, 30, 20 and 10 nm.

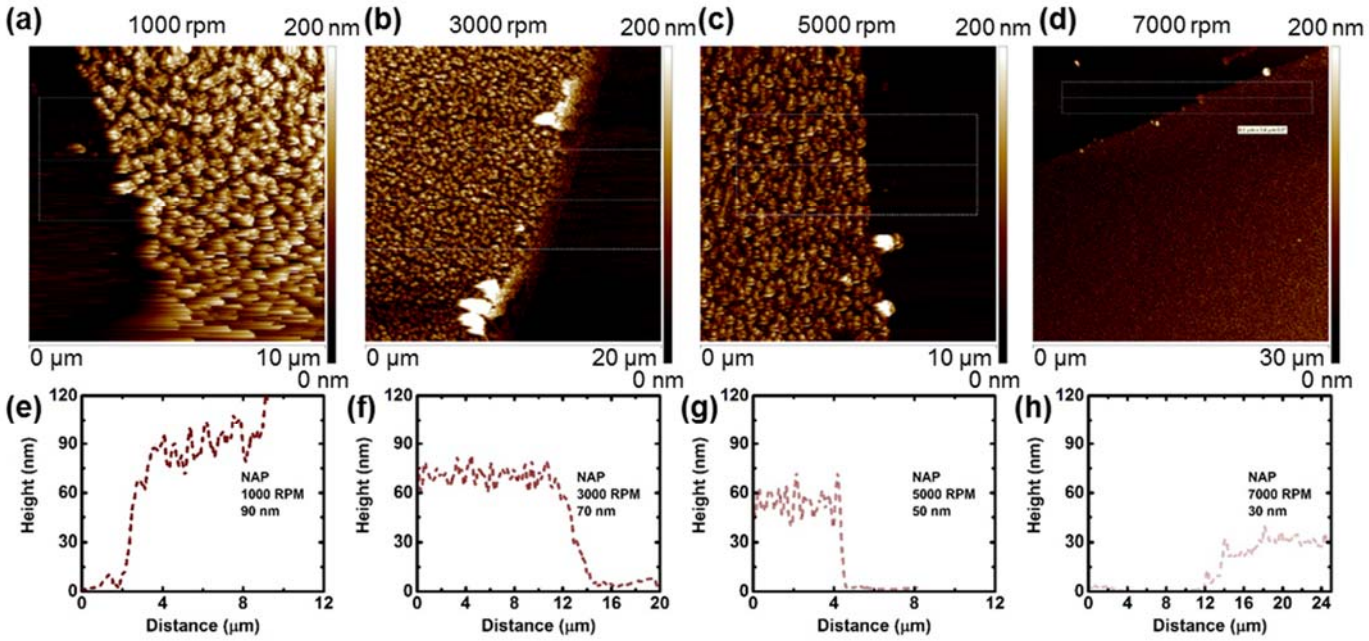

Figure S5: Topographical images ((a)-(d)) from AFM and plots of height versus distance ((e)-(h)) from the step function of NanoScope Analysis for the thickness measurement of NAP layers on Si with different spin speed from 1000 to 7000 rpm.

The thicknesses of NAP prepared by spin coating at 1000, 3000, 5000, and 7000 rpm are 90, 70, 50 and 30 nm, as shown in **Figure S5**.

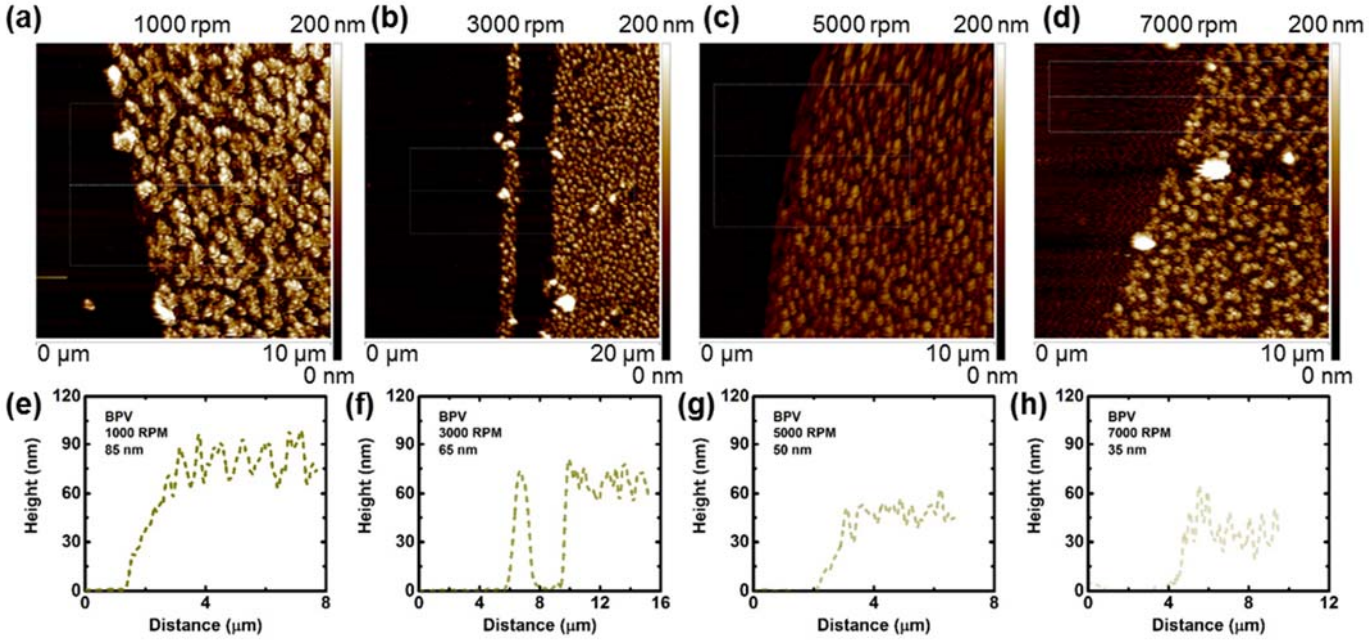

Figure S6: Topographical images ((a)-(d)) from AFM and plots of height versus distance ((e)-(h)) from the step function of NanoScope Analysis for the thickness measurement of BPV layers on Si with different spin speed from 1000 to 7000 rpm.

The thicknesses of BPV prepared by spin coating at 1000, 3000, 5000, and 7000 rpm are 85, 65, 50 and 35 nm, as shown in **Figure S6**.

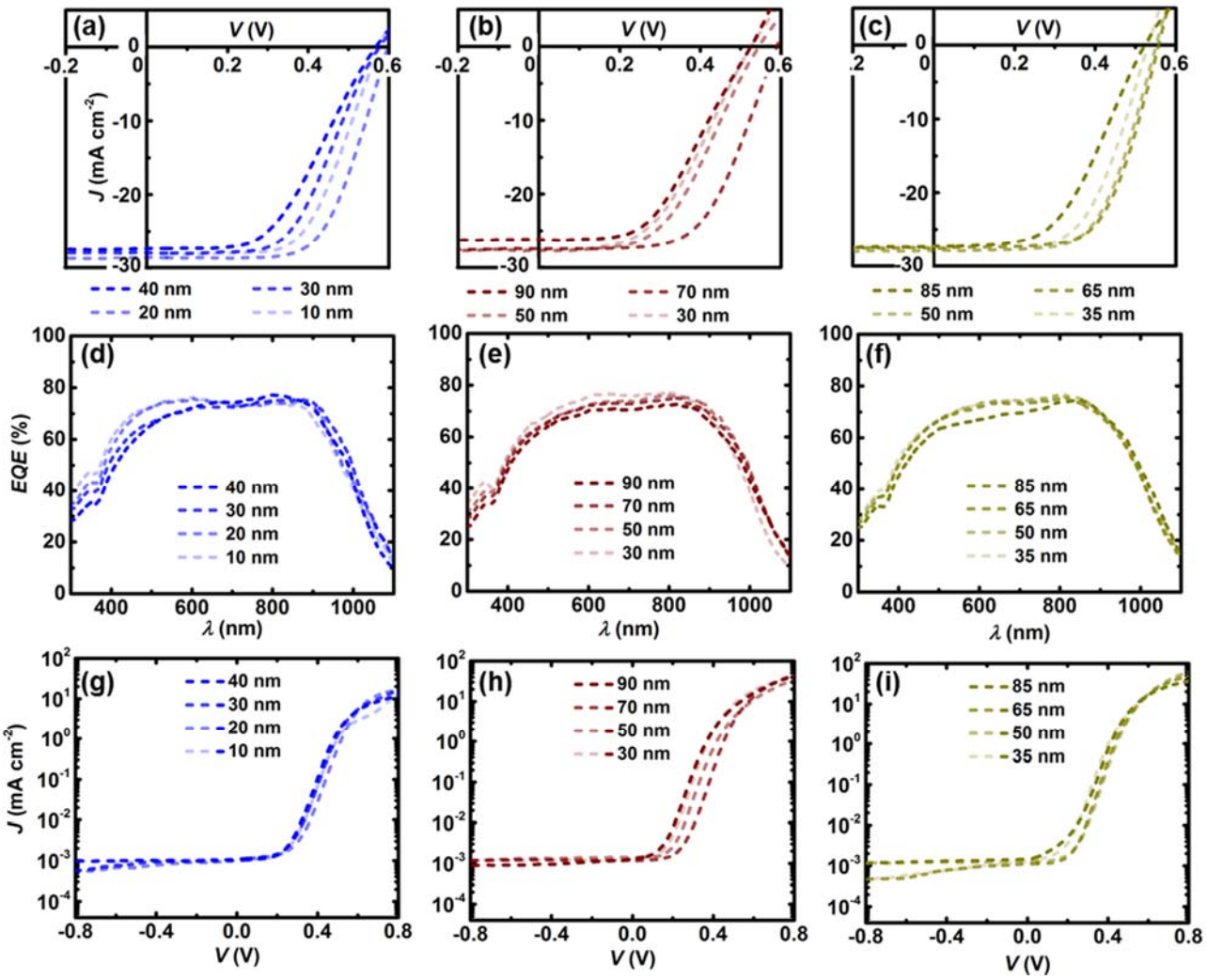

Figure S7: Performance of the GOCNT/HTL/Si devices with HTLs of different thicknesses: *J-V* curves under light conditions with (a) PEDOT:PSS, (b) NAP and (c) BPV as the HTL; *EQE* curves with (d) PEDOT:PSS, (e) NAP and (f) BPV as the HTL; *J-V* curves (*J* is on log scale) under dark conditions with (g) PEDOT:PSS, (h) NAP and (i) BPV as the HTL. The interlayers were applied with spin-coating at different speeds (1000, 3000, 5000, and 7000 rpm) and the thicknesses were measured by AFM and shown in each plot. All the devices in these plots are fabricated with as-prepared GOCNT films.

Figure S7 shows the *J-V* curves of GOCNT/HTL/Si devices with HTLs of different thicknesses (GOCNT/PEDO:PSS/Si, GOCNT/NAP/Si and GOCNT/BPV/Si) measured under both light and dark conditions as well as their *EQE* results. The details of these curves are summarised and plotted in **Figure 4** in the main text. Overall, 20 and 70 nm are the optimised thickness of PEDOT:PSS and NAP while GOCNT/BPV/Si devices seem to have high efficiency with the BPV thickness from 50 to 65 nm.

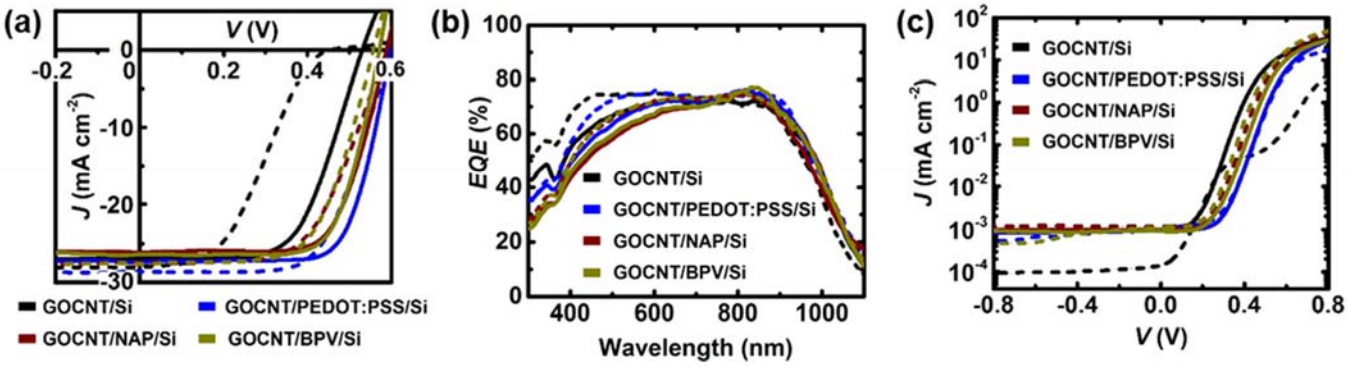

Figure S8: The influence of $AuCl_3$ doping on the solar cell (GOCNT/Si and GOCNT/HTL/Si with the optimised HTL thickness) performance; (a) *J-V* curves under light conditions; (b) *EQE* measurements; and (c) *J-V* curves under dark conditions. The short dash curves show the performance of the devices with as-prepared GOCNT films while the solid curves show the performance of the devices with $AuCl_3$-doped GOCNT films.

Figure S8 shows the impact of $AuCl_3$ doping on the performance of the GOCNT/Si and GOCNT/HTL/Si (with the optimised HTL thickness) devices. The details of these curves are summarised and showed in **Figure 5**. Overall, $AuCl_3$ doping is effective in improving all of the device performance parameters to varying degrees.